Energy Management Strategy of a PEM Fuel Cell Excavator with a Supercapacitor/Battery Hybrid Power Source

Tri Cuong Do [ID]**, Hoai Vu Anh Truong** [ID]**, Hoang Vu Dao, Cong Minh Ho, Xuan Dinh To, Tri Dung Dang and Kyoung Kwan Ahn *** [ID]

School of Mechanical Engineering, University of Ulsan, 93, Deahak-ro, Nam-gu, Ulsan 44610, Korea; cuongdt298@gmail.com (T.C.D.); truonganh241292@gmail.com (H.V.A.T.); hoangvudaocsp@gmail.com (H.V.D.); hocongminhck@gmail.com (C.M.H.); pageplan33286@gmail.com (X.D.T.); dangtridungs@gmail.com (T.D.D.)
* Correspondence: kkahn@ulsan.ac.kr; Tel.: +82-52-259-2282

Abstract: Construction machines are heavy-duty equipment and a major contributor to the environmental pollution. By using only electric motors instead of an internal combustion engine, the problems of low engine efficiency and air pollution can be solved. This paper proposed a novel energy management strategy for a PEM fuel cell excavator with a supercapacitor/battery hybrid power source. The fuel cell is the main power supply for most of the excavator workload while the battery/supercapacitor is the energy storage device, which supplies additional required power and recovers energy. The whole system model was built in a co-simulation environment, which is a combination of MATLAB/Simulink and AMESim software, where the fuel cell, battery, supercapacitor model, and the energy management algorithm were developed in a Simulink environment while the excavator model was designed in an AMESim environment. In this work, the energy management strategy was designed to concurrently account for power supply performance from the hybrid power sources as well as from fuel cells, and battery lifespan. The control design was proposed to distribute the power demand optimally from the excavator to the hybrid power sources in different working conditions. The simulation results were presented to demonstrate the good performance of the system. The effectiveness of the proposed energy management strategy was validated. Compared with the conventional strategies where the task requirements cannot be achieved or system stability cannot be accomplished, the proposed algorithms perfectly satisfied the working conditions.

Keywords: hybrid excavator; PEM fuel cell; supercapacitor; battery; energy management

1. Introduction

Nowadays, environmental pollution issues have become more serious and have caused bad effects on humans. One of the main reasons for this situation is the huge amount of emissions from transportation and construction vehicles. In particular, construction excavators (CEs) are widely used in many areas but they often consume a lot of fuel and produce large amounts of carbon gases. Hence, internal combustion engine (ICE) type excavators have recently been replaced by hybrid types in which good energy efficiency and fuel economy are satisfied [1–11]. However, this solution does not solve the problem completely and the emissions generated from the use of combustion engines are still a major problem to overcome.

A proton-exchange membrane fuel cell (PEMFC) power source is considered as a promising fossil-free power source for replacing the ICE. The chemical energy is directly converted into electrical energy by chemical reactions inside the fuel cell and releases pure water. Therefore, it achieves high

energy conversion efficiency, low operating temperature and pressure, and no environmental impact. However, using only a standalone fuel cell will decrease the lifetime of the system due to the slow dynamic response. Sudden changes of the operating load cannot be adopted and sufficiently supplied by PEMFC only. Besides, when the power supplied from the PEMFC exceeds the power demand or when the CEs are in regenerative operations, the PEMFC itself cannot store the excess energy. Therefore, the fuel cell (FC) system needs to be combined with other storage devices to maintain safety operation processes and to reduce costs. Some papers have used the combination between FCs and batteries (BATs) or supercapacitors (SCs) for excavators. Yi et al. [12] used a fuel cell excavator integrated with a BAT to complement the fuel cell, where he focused on only component sizing without considering energy management. Li et al. investigated a combination of the FC and the SC as the hybrid power source for an excavator [13]. Both the SC and the BAT are devices to store and release energy and to supply other devices. The BAT with high capacity, high efficiency and low energy leakage over time is expected to play an important role as an ideal electrochemical storage system in CE. However, when used at high power, losses during charging and discharging and the wear of the BAT increase. BAT is not enough for CE, where the power required changes suddenly and periodically.

Accordingly, to meet the load characteristics of CE, it is necessary to add an SC to the hybrid power supply to provide peak power in a short time. SCs are suitable for a large amount of power in a short time, and BATs are relatively suitable for storing a large amount of energy. Therefore, integrating BAT and SC with PEMFC improves performance, reduces system size, and improves fuel economy.

Some previous studies have investigated the fuel cell/BAT/SC hybrid power source configuration for electric vehicles (EVs) (i.e., cars) [14–22]. Their results have shown the benefit of this configuration for light vehicles. However, there are few works that investigate such combination of power sources for electric excavator systems. In this work, we extended our research work presented in [22], which was the first time that the integration of fuel cell/BAT/SC was applied to an electric excavator system. By the combination of three different devices, the hybrid power source becomes more complex and difficult to manage. Therefore, an appropriate energy management strategy (EMS) should be designed to effectively exploit the advantages of each device. The existing energy management strategies for various fuel cell vehicles can be mainly classified into optimization-based energy management strategies and rule-based energy management strategies.

The method relates to the theory of optimal control and consists mainly of the following two types: (1) global optimization energy management strategies such as dynamic programming (DP) [23] and Pontryagin's minimum principle (PMP) [24], and (2) real-time optimization energy management strategies such as the equivalent consumption minimization strategy (ECMS) [25] and model predictive control (MPC) [26]. The global optimization-based methods depend on the prior information of the driving cycles, so they cannot be implemented directly to a real-time control system. To reduce this gap, a real-time optimization-based strategy is needed. However, online tuning algorithms for parameters may result in computation burden. With the advantage of simplicity, robustness, and capability of real-time implementation, rule-based energy management methods have been widely utilized in many prototypes and commercial EVs. However, achieving optimal solutions using these EMSs is still a challenging problem.

Motivated by the above expressions, this paper proposes a novel energy management strategy for the hybrid PEMFC/BAT/SC hydraulics excavator (PEMFC-HE). The proposed energy management method was developed on the basis of an improved rules-based energy management strategy, which increases the efficiency of fuel cell systems and extends the life of hybrid power. In the proposed method, the fuel cell always operates in the optimal operating range, while the state of the charge (SOC) of the BAT and the SC is kept in an appropriate range. In addition, the operating mode and power distribution of the HE with the PEMFC/BAT/SC become clear. In order to apply the proposed EMS, mathematical models of the SC and BAT as well as dynamic models of PEMFC systems are presented. The simulation model of the hybrid power source is implemented in a MATLAB/Simulink environment, while the hydraulic model of the excavator is implemented in AMESim software. Models

of the entire system are built in a co-simulation environment, which is a combination simulation of AMESim and MATLAB/Simulink.

The main contributions of the paper are as follows:

(1) The FC–BAT–SC configuration is built into the CE for energy management. A new EMS strategy that considers all the working operations of the CE is introduced. This shows the effectiveness of the proposed algorithm in comparison with the existing algorithm.

(2) The model of the whole system, consisting of CE and integrated power supply, is represented in detail; the hydraulic model is implemented in AMESim, and the models of FC, BAT, and SC are simulated in a co-simulation environment in MATLAB/Simulink.

(3) The comparison of the proposed strategy with other existing strategies is carried out to verify the effectiveness of the integrated system with new goals.

The rest of the paper is organized as follows. The system components and its requirements are expressed in Section 2. The proposed energy management for the whole system is discussed in Section 3. The modeling of each component is derived clearly in Section 4 and then, in Section 5, some simulations are given to validate the proposed algorithm. Finally, conclusions as well as its potential applications are presented in Section 6.

2. System Components and Requirements

The structure of the PEMFC-HE is shown in Figure 1, where ICE is replaced by the hybrid power sources and the electric motors. The PEMFC-HE system consists of three parts: a hybrid power source, a powertrain, and a hydraulic system. The hydraulic system includes a boom, an arm, a bucket, and a swing mechanism, which are hydraulically driven by the hydraulic motor and cylinders. Flow from the main pump is distributed to each actuator by the control valve block. Besides, the powertrain system is driven by an electric motor, and FC, BAT and SC are integrated for the hybrid power source system. The energy flow in the PEMFC-HE is shown in Figure 2. The energy from the power sources with FC, BAT, and SC is supplied to the hydraulic system and the power train through three DC/DC converters, a DC bus, and electric motors. There are two types of DC/DC converters in the PEMFC-HE system. A boost DC/DC converter is employed to connect the FC to the DC bus, while two bidirectional DC/DC converters are utilized to connect the BAT and SC to the DC bus, which enables energy to flow in both directions. Moreover, the PEMFC-HE structure can have an energy regeneration part that can recover energy from the boom cylinder as it moves down by the gravitation force or braking energy during the swing stage. However, it makes the system more complex and expensive. Therefore, the potential energy recovery will be investigated in our future work.

CE performs many heavy tasks such as lifting, dumping, rotating, braking, and other auxiliary functions. Hence, the demanded power from the FC/BAT/SC sources varies depending on the working patterns. It can be divided into four cases: (1) low power, (2) medium power, (3) high power for doing a single task, and (4) very high power for doing multi tasks.

Low power is required in a case where the CEs move to a new position, lift the arm up without load by boom cylinder or arm cylinder, and brake the system when it stops working. Therefore, the required power is low and not immediate. Medium power is required when the CEs are going uphill, slowly braking when arriving at the destination angle, scooping the loads that are not so heavy. The power demand in these cases is not too high and can be supported by adding another component to enhance the total power. High power is required in the case of handling an objective which is very heavy, such as stone or concrete. If the CE is working, but encounters obstacles to crush in the process, the actuator must be driven at high power for the requested operation. When a CE performs a complex task, it requires a large amount of power. The CEs are lifting and swinging at high inertia at the same time, lifting and braking in case of emergency, or lifting and moving to a high position. In this case, very high power is required immediately. Therefore, the energy sources and EMS need to be designed and selected to satisfy the above requirements.
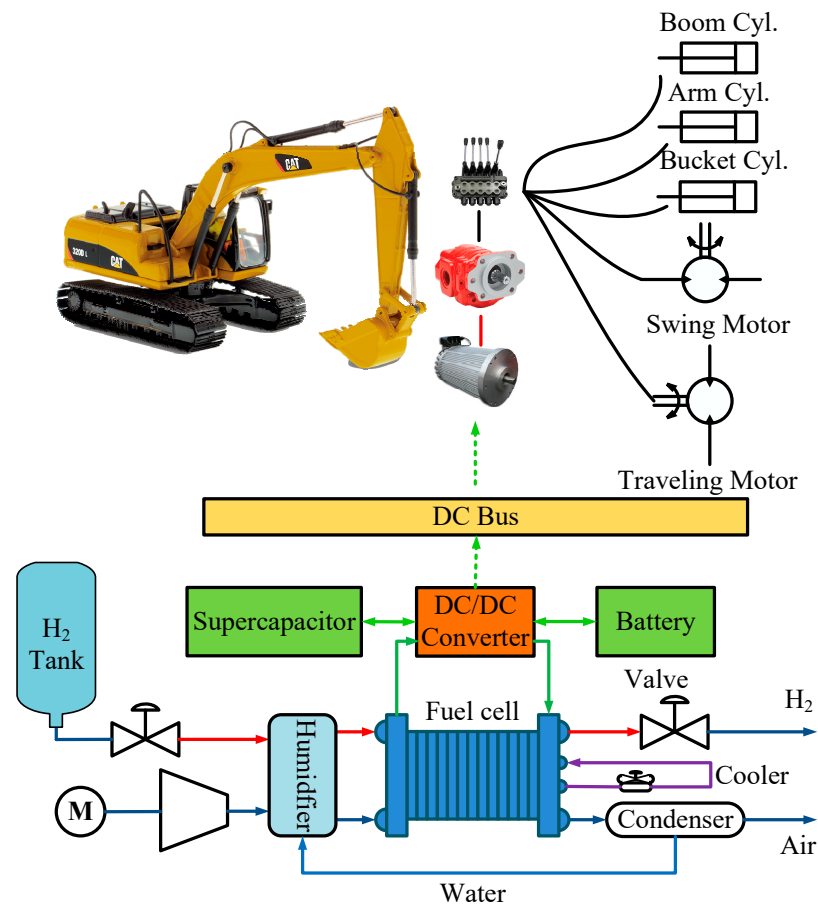
Figure 1. Proton-exchange membrane fuel cell-hydraulics excavator (PEMFC-HE) structure.
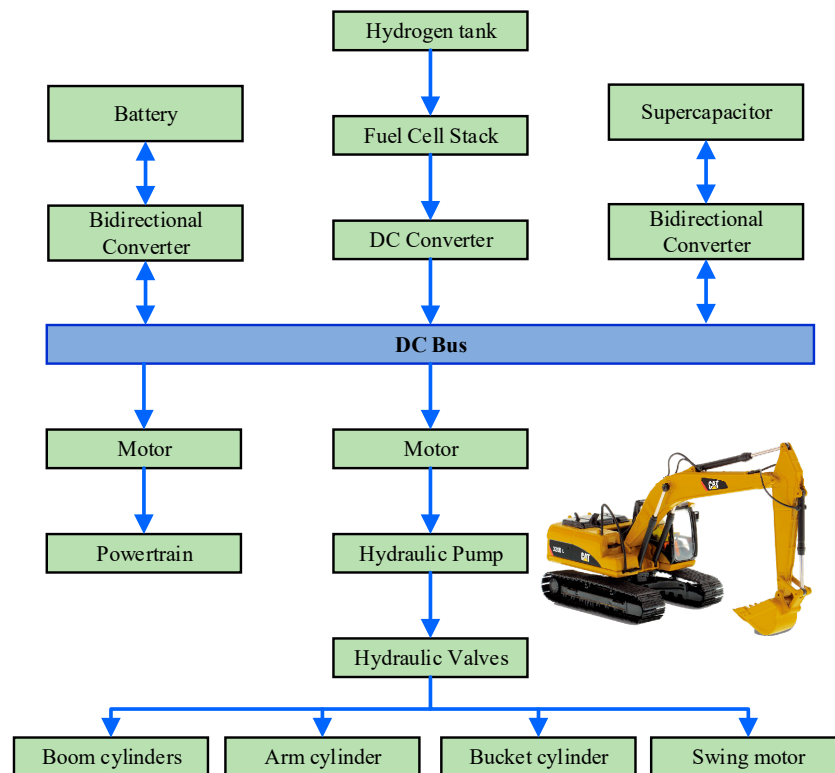

Figure 2. Energy flow of the proposed PEMFC-HE.

Based on the above analysis, we proposed a combination FC system with the SC and BAT as a hybrid power source to run the CEs. The FC is utilized as the main power supply. The SC and BAT are equipped to boost the system in case of the higher demanded power. There are some different potential applications between them due to their distinct characteristics and structure. The BAT is structured from the chemical unit and stores its potential power in a chemical form. Hence, the BAT can store large amounts of energy. However, a discharge (or charge) process is a result of a chemical reaction that needs a long time to transfer the chemical energy into electrical energy (or vice versa). Therefore, the BAT cannot respond fast enough when changing current to release high power. Different from the BAT, the potential power in the SC is stored in an electric field that allows the SC to rapidly discharge (or charge) and supply power immediately to other devices, depending directly on the conduction capabilities of the capacitor plates. Besides, high power can be achieved due to very high capacitance of the SC compared with the BAT. The life cycle of the SC is also longer than the BAT, but performance is limited to low voltage (high voltage would damage the SC). Hence the SC is suitable for use when large power is required to be achieved in a very short time. Based on the above analysis, the using of SC-BAT is more effective than using each component separately, thus increasing workability and system performance.

3. Proposed Energy Management Strategy

3.1. Conventional EMS

3.1.1. Conventional EMS-A

The design of the conventional EMS-A [16,17,19] for the powertrain is shown in Figure 3. In this diagram, P_{req} and P_{fc} denote the power required from the powertrain and the power induced from the fuel cell, respectively; SOC_{bat} and SOC_{SC} denote the state of charge of the BAT and SC, respectively. The minimum state of charges of the BAT and the SC are defined as SOC_{bat_min} and SOC_{sc_min}, respectively [16,17,19].

In this EMS, the required power is firstly checked. If the required power is negative, then the system is braked, and no power is needed. However, if the required power P_{req} is positive but smaller than power of the fuel cell P_{fc}, the FC will individually supply power to the PEMFC-HE. On the other hand, if the required power P_{req} is larger than P_{fc}, then the FC extracts the nominal power and the remainder is supplied from the SC first. In the case that P_{req} exceeds the maximum power of the FC and SC combined, the BAT must discharge. During the operation, the SOCs of the BAT and the SC are monitored and kept in suitable ranges. In addition, when the required power P_{req} is lower than P_{fc} and the vehicle is braking, the power of the FC is supplied to satisfy the required power and charge the SC or BAT. The priority of charging process for the SC and BAT is designed as the following principle: the prior charging power is delivered to the BAT in the weak deceleration, and to the SC in the strong deceleration. However, this EMS appears to have no means of recharging the BAT or SC. Therefore, it has a very limited time for which it can operate, especially in long term working vehicles.
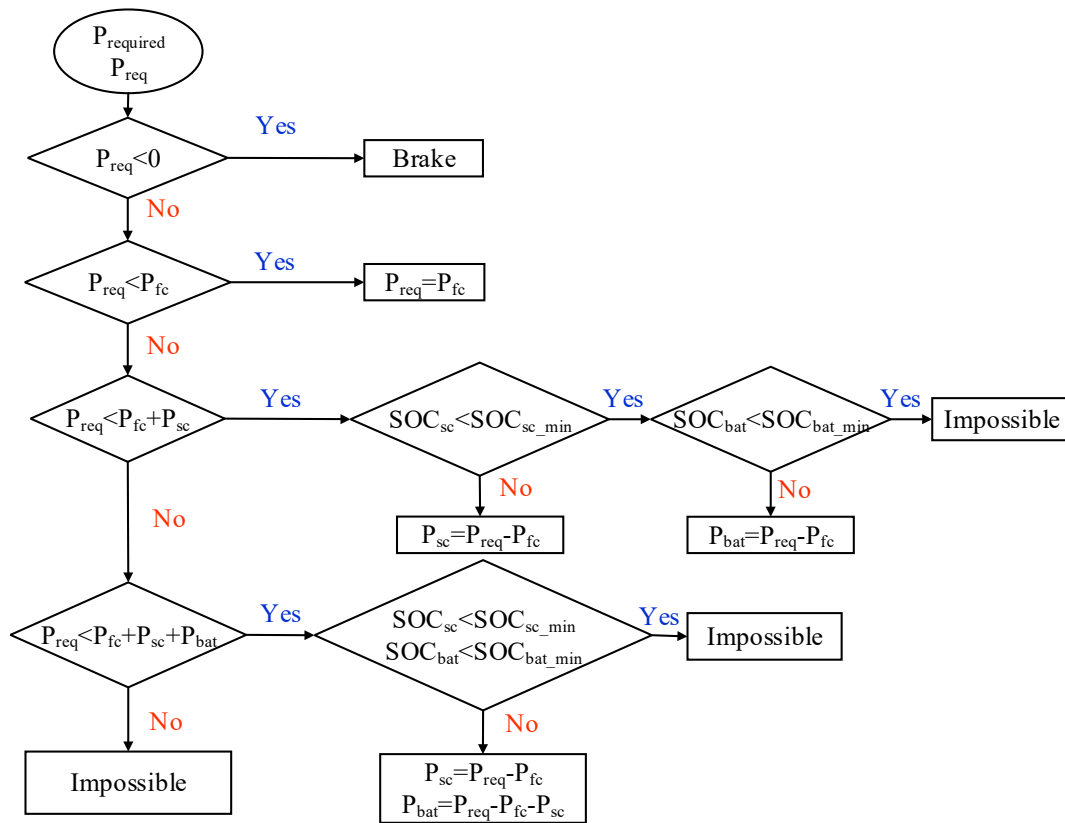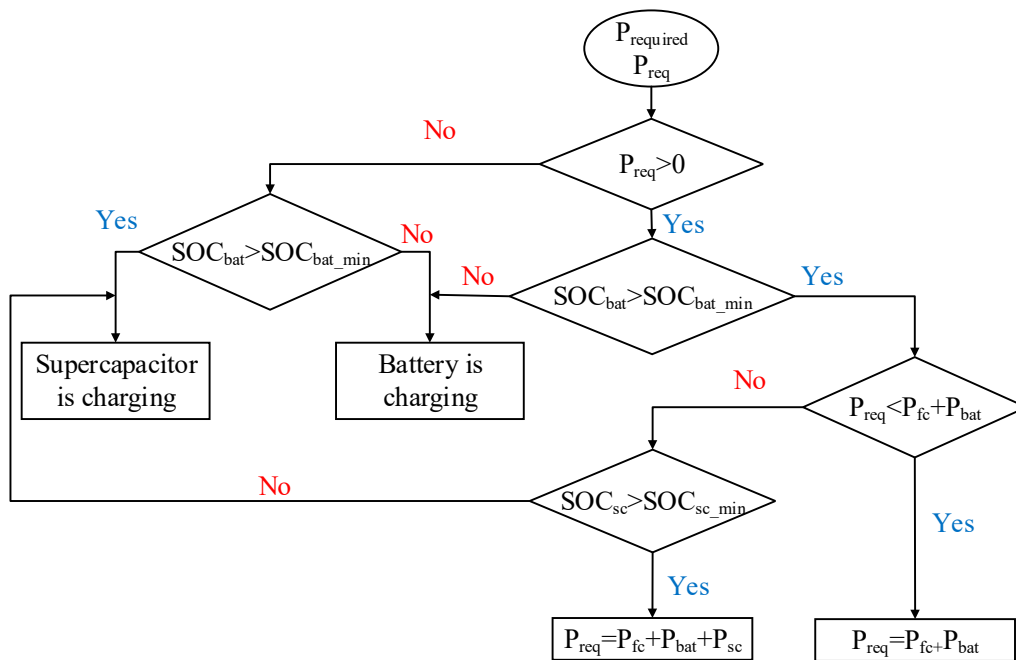
Figure 3. The flowchart of the power systems [16,17,19].

3.1.2. Conventional EMS-B: For Hydrogen Fuel Saving in the Hydrogen Fuel Cell Vehicles

In the work presented in [18], the objective of the control strategy was to decrease the fuel consumption of the fuel cell by integrating a BAT and SC into the system, as shown in Figure 4. Based on the properties of the BAT, the value of SOC_{bat} is kept between 60% and 90%. During the operation, SOC_{bat} will be checked. If SOC_{bat} is greater than SOC_{bat_min}, the FC and BAT is combined to drive the vehicle. The SC, which is the fastest energy source, is employed to supply power for the vehicle in the case of sudden and high-power requirements. In the regeneration mode ($P_{req} < 0$), if SOC_{bat} is smaller than its lower limit SOC_{bat_min}, the BAT will be charged. Similarly, the SC is charged if SOC_{SC} is smaller than SOC_{SC_min}. In the case that power demand exceeds the maximum power of the FC and BAT combined and SOC_{SC} is larger than SOC_{SC_min}, the FC and BAT provide the required power with their maximum power and the SC provides the surplus power demand.

This EMS has some drawbacks, as in the following. First, if the SOC_{bat} is lower than its lower limit SOC_{bat_min}, the FC has to charge to the BAT first, which delays the power delivery process. The same problem occurs in the case where SOC_{SC} is lower than its lower limit SOC_{SC_min}. Besides, when the BAT is charged, if the FC does not have enough power to satisfy the power demand, then the BAT has to suddenly change from charge mode to discharge mode. In this time, the SOC_{bat} will be decreased and lower than the minimum threshold, then the FC must charge the BAT again. This process can lead to an unstable system that decreases the lifetime of the devices.

Figure 4. The flowchart of hydrogen fuel saving control strategy (HFS-CS) [18].

3.1.3. Conventional EMS-C: Extend the Life Cycle in the Hydrogen Fuel Cell Vehicles

The objective of this EMS is to extend the life cycle of the BAT and SC [18]. To meet this requirement, only power generated from the FC delivers to the vehicle when it runs on a straight road, and there is no high or sudden peak power requested. The BAT and SC are only included in the system as assistant supplies if the vehicle requires more power as it moves uphill or accelerates. The regenerative braking energy is delivered to the SC during sudden and rapid braking or to the BAT in the case of weak and slow braking.

As can be obtained from the flowchart control in Figure 5, If P_{req} is negative, the vehicle is in the regeneration mode. The SC is firstly charged if the SOC_{SC} is lower than SOC_{SCmin}. Otherwise, the BAT will be charged first. If P_{req} is positive, the relationship between P_{req} and the power of the FC is considered first. If the power of the FC can satisfy the power demand, it provides energy to the vehicle. If the power demand is greater than the P_{fc}, the FC delivers its maximum power and the SC delivers the remaining power demand. When P_{req} exceeds the maximum power of FC and SC combined, the BAT must discharge and provide the surplus power demand. As claimed by the author, the life cycle of the energy storage technologies is improved.

Although good results were obtained using this EMS, there are some issues that need to be discussed. In this strategy, the SC is firstly used when the P_{req} exceeds the FC power. This can lead to two problems. The first problem occurs in the case that SOC_{SC} is lower than its lower limit SOC_{SC_min} and the P_{req} is greater than the maximum power of the FC. As mentioned in the EMS-B, the problem leads to the shortage of the supplied power to the vehicle or a reduction in the lifetime of the devices. The second issue arises when the BAT is always charged as long as the SOC_{SC} is greater than the minimum level. Thus, an overcharging phenomenon of the BAT occurs and the efficiency of the system is reduced.
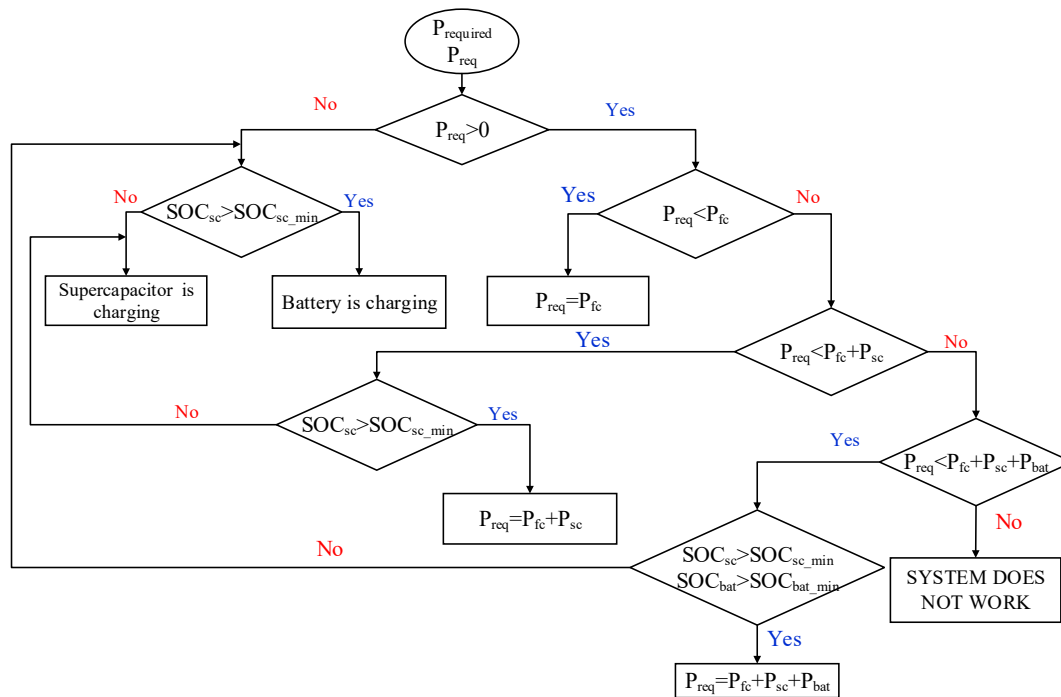
$P_{required}$
P_{req}

$P_{req} > 0$ — No / Yes

$SOC_{sc} > SOC_{sc\_min}$ — No / Yes

$P_{req} < P_{fc}$ — Yes / No

Supercapacitor is charging

Battery is charging

$P_{req} = P_{fc}$

$P_{req} < P_{fc} + P_{sc}$ — Yes / No

$SOC_{sc} > SOC_{sc\_min}$ — No / Yes

$P_{req} < P_{fc} + P_{sc} + P_{bat}$ — Yes / No

$P_{req} = P_{fc} + P_{sc}$

$SOC_{sc} > SOC_{sc\_min}$
$SOC_{bat} > SOC_{bat\_min}$ — Yes / No

SYSTEM DOES NOT WORK

$P_{req} = P_{fc} + P_{sc} + P_{bat}$

Figure 5. The flowchart of life cycle saving control strategy (LCS-CS)) [18].

3.2. Proposed EMS

When using the hybrid power source (HPS), the working principle and operation modes of the HPS should be optimize as it saves energy and increases the lifetime of the components. Based on the characteristics of each device and demanded working conditions of the excavator, the proposed algorithm for operating modes is given in Figure 6.

The level of the power demand is determined depending on the working conditions and movement of elements. Basically, the power measured from the system movement is utilized as a reference for choosing devices and designing the EMS. Therefore, firstly, the power required from the system is pre-defined, as shown in Figure 7. The fuel cell is reasonably chosen such that "high power and good efficiency can be satisfied with the acceptable number of stacks". The remain power is distributed for the battery and supercapacitor.

If the fuel cell itself can satisfy the requirement, then the power demand at that event is determined as low power demand.

If the requirement exceeds the power supplied from the fuel cell, but is still less than the sum of power from the fuel cell and supercapacitor, then the power demand is determined as high power or medium power depending on which auxiliary device the remain power demand is boosted from.

If the fuel cell and battery can supply sufficient power to the system, then the power demand at that event is determined as medium power.

If the fuel cell and battery cannot satisfy the requirement but the fuel cell and supercapacitor can adapt to the requirement, then the power demand is determined as high power.

If the power demand requires power from all devices (fuel cell and battery and supercapacitor), then it is determined as very high power.

Case 1: Low Load Power is Required.

If the P_{req} is less than the nominal power of the FC (P_{fc_n}) ($P_{req} \leq 0.8P_{fc\_n}$), then the electric power generated from the FC is supplied primarily. Besides, extra energy from the FC is used to charge the SC or BAT if needed. (During the charging mode, if the state of charge SOC_{bat}/SOC_{SC} reaches the maximum value ($SOC_{bat}/SOC_{SC} = SOC_{MAX}$), the charging is stopped). Otherwise, the nominal power

is supplied from the fuel cell, and the remainder is supported from the SC or BAT, depending on the particular working conditions.
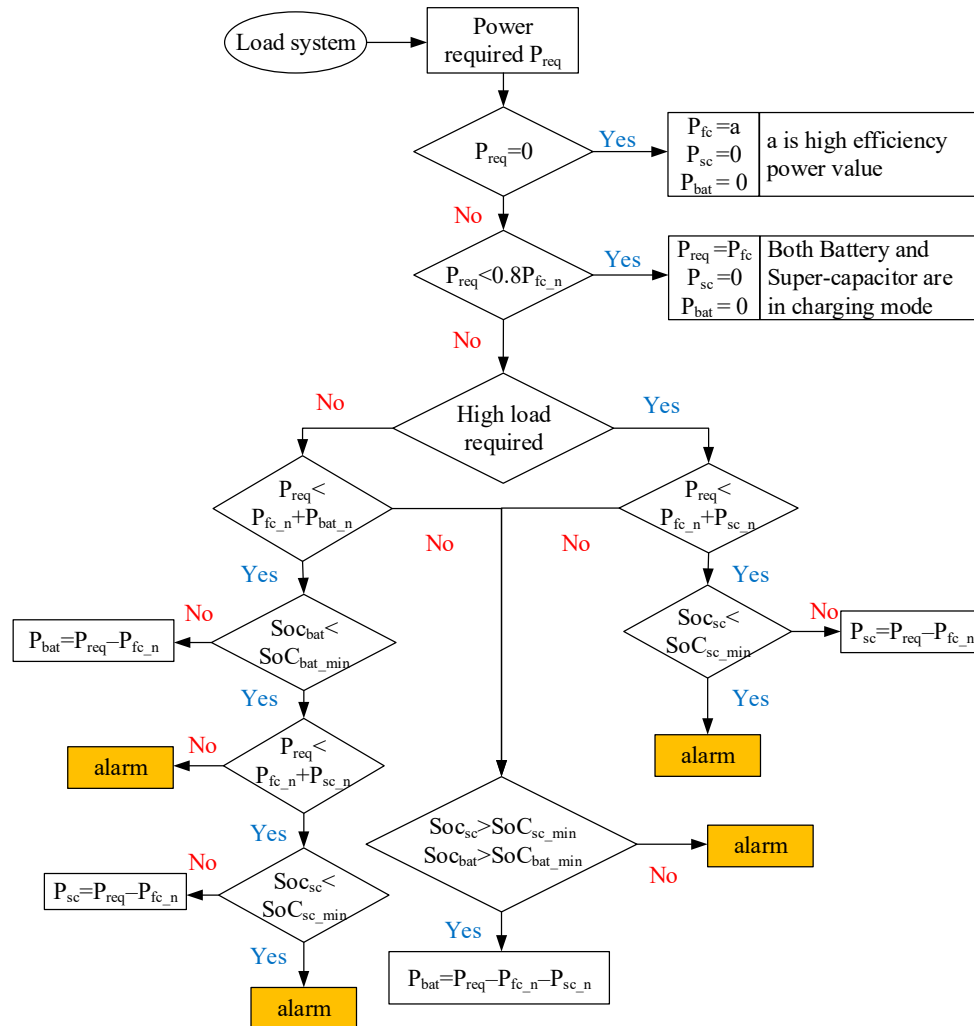
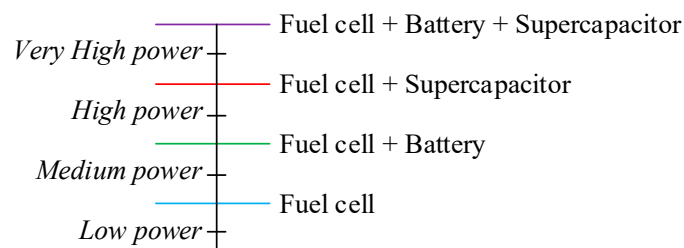**Figure 6.** The flow chart of the proposed algorithm.

Figure 7. The level of the power demand.

Case 2: Medium load power is required.

In case of the medium load power, the remained power can be supplied from the BAT first. Using the same procedure as the first case, the SOC_{bat} should be maintained within an acceptable range during operation. If the BAT is fully discharged, then the SC can replace it and provide power if needed.

Case 3: High load power is required.

In this case, the remaining P_{req} is boosted from the SC due to its ability. During the operation of this mode, the SOC_{SC} should be regulated in a range of the state of charge ($SOC_{SC} > SOC_{SC\_min}$). When the SOC_{SC} is less than the limitation, the SC is fully discharged and cannot provide more power for the circuit and is replaced by the power discharged from the BAT. Same as the SC, the SOC_{bat} should be kept within an acceptable range ($SOC_{bat} > SOC_{bat\_min}$). If the BAT is fully discharged ($SOC_{bat} < SOC_{bat\_min}$), then no more power can be gotten from the BAT. In this case, an "alarm" notification is switched on for warning that the SC and BAT need charging.

Case 4: Very high load power is required.

If P_{req} exceeds the total nominal power of both the fuel cell and the SC ($P_{req} > P_{FC\_n} + P_{SC}$), the BAT enters the circuit. While performing, both SOC_{SC} and SOC_{bat} should be maintained in the acceptable range ($SOC_{SC} > SOC_{SC\_min}$ and $SOC_{bat} > SoC_{bat\_min}$). Otherwise, unexpected conditions may happen in the control unit that affects the system. Therefore, both the SC and BAT must be properly charged to optimize working conditions. To prolong the lifetime of the BAT and SC, the maximum SOC of both devices is selected to be 0.9. When the SOC is charged higher than this value, the charging process will stop. The minimum SOC of the SC is 0.3 while for the BAT it is 0.6. If the SOC of each device is lower than these values, the discharging mode will stop.

Compared with the conventional algorithm depicted in Section 3.1, we considered that the use of the SC or BAT with the fuel cell depends on the requested tasks to minimize wasted energy as well as to increase efficiency and the lifetime of the components.

4. System Modeling

4.1. Fuel Cell Model

4.1.1. Electrochemical Model

A simplified model of the fuel cell is presented as Figure 8. The output voltage of a single fuel cell can be defined by the following equation [22,27–29]:

$$V_{cell} = E_{Nernst} - V_{act} - V_{conc} - V_{ohmic} \tag{1}$$

where: E_{Nernst}, V_{act}, V_{conc} and V_{ohmic} are the thermodynamic potential, activation voltage loss, concentration voltage loss, and ohmic voltage loss, respectively.
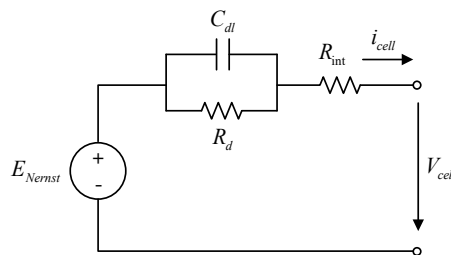

Figure 8. A simplified model of the fuel cell.

The Nernst equation for reversible thermodynamic potential is displayed as following:

$$E_{Nernst} = 1.229 - 8.5 \times 10^{-4}(T - 298.15) + \frac{RT}{2F} \ln\left[p'_{H_2}(p'_{O_2})^{0.5}\right] \tag{2}$$

where: p'_{H_2}, p'_{O_2}, T, R, F represent the hydrogen and oxygen partial pressure, cell temperature, the universal gas constant, and Faraday constant, respectively.

The ohmic voltage loss of the system caused by the internal resistance of the electrolyte membrane is calculated as the following equation:

$$V_{ohmic} = iR_{int} \tag{3}$$

At low current densities, the activation voltage loss is responsible for the main drop of fuel cell voltage and it can be described as the equation below:

$$V_{act} = \xi_1 + \xi_2 T + \xi_3 T \ln\left(c'_{O2}\right) + \xi_4 T \ln(i) \tag{4}$$

where R_{int}, is the internal resistance of the electrolyte membrane, c'_{O2} is the oxygen concentration at the cathode/membrane interface, $\xi_1 \ldots \xi_4$ are parametric coefficients, and i is the cell current.

During the electrochemical reaction at the electrode surface, the reactant concentration change causes the voltage loss which is calculated as ([30])

$$V_{conc} = \frac{RT}{nF} \ln\left(\frac{(i/A)_L}{(i/A)_L - (i/A)}\right) \tag{5}$$

Due to the double capacitor layers effect at the electrode-electrolyte interface, the voltage drop can be computed as ([31])

$$\frac{dV_d}{dt} = \frac{i}{C_{dl}} - \frac{V_d}{R_d C_{dl}} \tag{6}$$

where R_d denotes the sum of activation resistance and concentration resistance, and V_d is the voltage drop [31].

$$R_d = \frac{V_{act} + V_{conc}}{i} \tag{7}$$

Considering all aforementioned effects, the voltage of a single cell can be computed as

$$V_{cell} = E_{Nernst} - V_d - V_{ohmic} \tag{8}$$

The total voltage is created by combining the number of cell N, as below:

$$V_{stack} = NV_{cell} \tag{9}$$

4.1.2. Reactant Flow Model

The reactant flow model for the anode is given by the following equation:

$$\frac{V_a}{RT} \frac{dp'_{H_2}}{dt} = \dot{m}_{H_2,in} - \dot{m}_{H_2,out} - \frac{Ni}{2F} \tag{10}$$

where with $V_a, \dot{m}_{H_2,in}, \dot{m}_{H_2,out}$ are the anode volume, hydrogen inlet, and hydrogen outlet flow rates through the fuel cell stack, respectively.

The hydrogen outlet flow rates through fuel cell stack is given by

$$\dot{m}_{H_2,out} = k_a\left(p'_{H_2} - p_{\tan nk}\right) \tag{11}$$

where k_a is a flow constant for the anode, $p_{\tan nk}$ is the pressure of the hydrogen tank.

Similar to the cathode, we have

$$\frac{V_c}{RT} \frac{dp'_{O_2}}{dt} = \dot{m}_{O_2,in} - \dot{m}_{O_2,out} - \frac{Ni}{4F} \tag{12}$$

where $V_c, \dot{m}_{O_2,in}, \dot{m}_{O_2,out}$ are the cathode volume, oxygen inlet, and oxygen outlet flow rates through the fuel cell stack, respectively.

$$\dot{m}_{O_2,out} = k_c\left(p'_{O_2} - p_{BPR}\right) \tag{13}$$

The total power input of the system is proportional to the amount of hydrogen consumed.

$$P_{tot} = \dot{m}_{H_2,used}\Delta H = \frac{Ni}{2F}\Delta H \tag{14}$$

where ΔH is the enthalpy of combustion for hydrogen.

Finally, the electrical output power is

$$P_{elec} = V_{stack}i \tag{15}$$

4.2. Supercapacitor Model

The SC is chosen as a secondary unit to supply power because of its advantages such as high-power density, high power release, fast charge and discharge. Without using the SC, the FC and BATs have to fulfill all required power even when high peak power occurs, thus degrading performance, lifetime, or increasing the size and costs in a trade-off [32]. For the equivalent model of the SC, see [33,34]. The SC, in general, composes of capacitors, resistors representing the charging or discharging units. The unit cell of the SC is constructed with two RC branches in parallel, as described in Figure 9 [35].

The immediate branch R_1C_1 in the main cell specifies the fast response during the charge or discharge process in a short time [36]. After completing the charge mode, all charge is in the capacitor C_1 of the immediate branch. Then, the charge redistributes itself to the second branch R_2C_2 in the slow cell. The resistor R_f represents the leakage behavior and can be simply ignored since the leakage current is equal to a few milliamps in a big SC.

The energy stored in the SCs at the voltage U_{SC} is derived as

$$E_{sc} = \frac{1}{2}C_{eq}U_{sc}^2 = \frac{1}{2}\frac{N_{p\_sc}}{N_{s\_sc}}C_{sc}U_{sc}^2 \tag{16}$$

where C_{eq} is an equivalent capacity of the SCs, N_{p_sc} and N_{s_sc} denote the parallel branches and the serial connection of the SCs, respectively; C_{sc} is the SC capacitance.
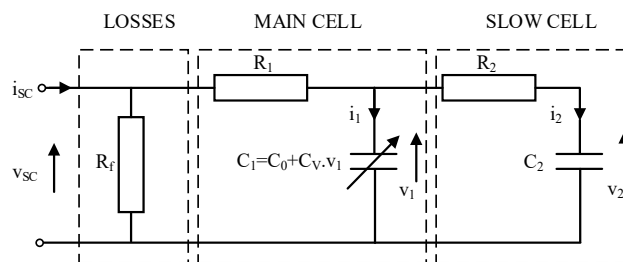

Figure 9. A simplified model of the supercapacitor.

The voltage of the SC can be obtained through the calculation of a single pack as follows:

$$U_{sc} = N_{s\_sc}\left(v_1 + R_1\frac{I_{sc}}{N_{p\_sc}}\right) \tag{17}$$

where U_{sc} and I_{sc} are the voltage and current of the pack supercapacitor, respectively; v_{sc} and i_{sc} are the voltage and current of an elementary SC, respectively.

The voltage of secondary capacity C_2 is calculated as a non-linear function of capacitance C_2 and resistance R_2:

$$v_2 = \frac{1}{C_2}\int \frac{1}{R_2}(v_1 - v_2)\mathrm{d}t \tag{18}$$

The change rate of an instantaneous charge of C_2 is proportional to the current i_2 as

$$\frac{\mathrm{d}}{\mathrm{d}t}Q_2 = i_2(t) \tag{19}$$

The current of the main capacitor can be calculated as the function of the capacity Q_1:

$$i_1 = C_1\frac{\mathrm{d}v_1}{\mathrm{d}t} = \frac{\mathrm{d}Q_1}{\mathrm{d}t} = (C_0 + C_v v_1)\frac{\mathrm{d}v_1}{\mathrm{d}t} \tag{20}$$

where the charge Q_1 is calculated through the equivalent C_1 and voltage dropped on this unit as

$$Q_1 = C_0 v_1 + \frac{1}{2}C_v v_1^2 \tag{21}$$

From this, one can obtain the voltage of the v_1 as

$$v_1 = \frac{-C_0 + \sqrt{C_0^2 + 2C_v Q_1}}{C_v} \tag{22}$$

Finally, the SOC_{SC} is calculated as the ratio between the current SC capacity and the maximum SC capacity.

$$SOC_{SC} = \frac{1}{Q_{\max}}\int_{t_0}^{t} I_{SC}(\tau)\mathrm{d}\tau \tag{23}$$

where I_{SC} is the charging current, $Q_{\max}$ is the maximum capacity of the SC.

The SOC_{SC} should be considered as an important factor to evaluate the state of the SC bank.

4.3. Battery Model

The BAT is considered as another second unit functioning as the buffer supply for the system when the FC cannot adapt to the power demand during an endurance operation, as shown in Figure 10. For designing the EMS, the model of the BAT should be established with some invoked parameters to assess working status, thereby giving criterions for effectively designing EMS. The model of the battery can be revealed in the literature [37–39]. In this study, the BAT is simply derived for the aim of EMS design as follows:

The controlled voltage source is described by ([40])

$$E = E_0 - K\frac{Q_{\max}}{Q} + Ae^{B(Q-Q_{\max})} \tag{24}$$

The battery voltage is computed as

$$V_{bat} = E - Ri \tag{25}$$

where $Q_{\max}$ denotes the maximum capacity of the BAT, A is the exponential voltage, B is the exponential capacity of the BAT, E_0 is the voltage in case of no load, K is the polarized voltage constant, and R is the BAT resistor.

The BAT voltage, in another view, relates to the BAT state of charge (SOC_{bat}). Then Equation (24) can be rewritten as ([14])

$$E = E_0 - K\frac{1}{SOC_{bat}} + Ae^{BQ_{\max}(SOC_{bat}-1)} \tag{26}$$

For the discharge process, the energy released from the BAT is calculated as

$$E_{release} = E_0 - K\frac{1}{SOC_{bat}} \times it - Ri + Ae^{BQ_{max}(SOC_{bat}-1)} - K\frac{1}{SOC_{bat}} \times i^* \tag{27}$$

where i^* is the filtered current at low frequency, and t is time parameterized.

The BAT output power is expressed as

$$P_{bat} = V_{bat}i \tag{28}$$

The state of charge of the BAT (SOC_{bat}) can be derived from the current charge and the maximum charge of it.

$$SOC = \frac{Q_{max} - it}{Q_{max}} \tag{29}$$

The SOC_{bat} is another important parameter, together with the SOC_{SC}, that reflects the status of the devices and is invoked to evaluate how much energy left for use.
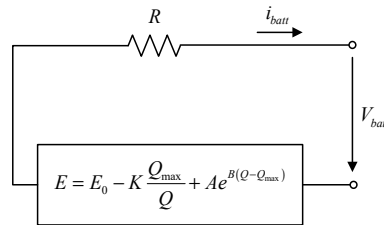

Figure 10. Battery equivalent circuit.

4.4. DC/DC Converter Model

The fuel cell system is connected to a boost DC-DC converter while the BAT and SC are linked to the DC bus with two corresponding bidirectional DC-DC converters. These DC-DC converters are used to transfer the electric energy between the low voltage power sources and the high voltage load, as shown in Figure 11. In addition, the two bi-direction DC-DC converters are required for both delivery and recovery cycles. Since energy management is at a higher layer than local control and different layers should be treated by different operating frequencies, it is supposed that the time constant of the inductor is much greater than the switching period of the DC-DC converter and the modulation frequency is sufficiently high to consider an average model [41]. Moreover, once the inner-loop subsystem is well controlled, it is assumed to respond immediately to the reference. Thus, it is necessary to reduce the fast dynamics of the DC-DC converter by the following equivalent static model [42,43]

$$V_I - V_h = L\frac{di_L}{dt} + i_L R_L \tag{30}$$

$$V_h = \kappa V_O \tag{31}$$

$$i_O = \kappa i_L \eta^\beta$$
$$\begin{cases} \beta = 1, & \text{for boost converter or for} \\ & \text{bidirectional converter with } i_O V_O \geq 0 \\ \beta = -1, & \text{for bidirectional converter with } i_O V_O < 0 \end{cases} \tag{32}$$

where V_I, V_O are the input voltage and output voltage of the DC-DC converter, respectively; L and R_L are the inductance and the resistor of the inductor, respectively; κ is the ratio of output voltage and input voltage of the converter, i_L and i_O are the current through inductor and the output current of the converter, respectively; and η is the efficient of the converter.
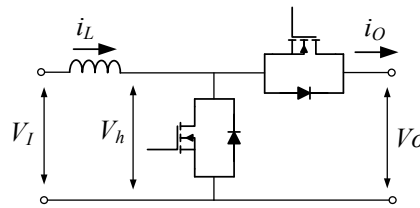
Figure 11. DC/DC converter electric circuit.

4.5. Excavator Hydraulic Model

The outlet pressure and flow rate of the hydraulic pumps can be used to calculate the power demand of the hydraulic system P_p, as follows ([44,45]):

$$P_p = \frac{p(t) \times q \times n(t)}{600 \times \eta(t)} \tag{33}$$

where p, q, η, and n denote the pressure, displacement, efficiency, and rotational speed of the hydraulic pump, respectively. The energy–balance equations are established for the electrical motors considering their operational efficiency. The power demand of the electric motor can be estimated as follows:

$$P_M = \frac{P_p}{\eta_M} \tag{34}$$

where P_M is the power demand of the motor driving the hydraulic pump; η_M denotes the working efficiency of the motor.

5. Simulation Results and Discussion

To fully evaluate the effectiveness of the proposed control strategy presented in Section 3.2, the performance of HPS supply to the HE was verified by the simulation method. The simulations were conducted by using a co-simulation between AMESim 15.2 (version 15.2, Siemens company, Dalas, TX, USA) and MATLAB 2017a (version 2017a, MathWorks company, Natick, MA, USA) with a sampling time of 10 ms, as presented in Figure 12; Figure 13. LMS AMESim, which has been known as a strong tool for dynamic simulations of hydraulic systems, was used to simulate a configuration of the HE with the real parameters, as shown in Table 1. Besides, a combination model of FC, SC and BAT was built in MATLAB/Simulink according to the mathematical equations. With the adaptive programming of MATLAB, it was easily combined with LMS AMESim for specific responsibilities of the simulation via S-Function.

Table 1. Parameters for the excavator model.

Component	Value	Unit
Boom cylinder (Piston diameter × Rod diameter × Stroke length)	$0.35 \times 0.22 \times 1.8$	m
Arm cylinder	$0.18 \times 0.125 \times 1.7$	m
Bucket cylinder	$0.21 \times 0.13 \times 1.33$	m

In this research, the working cycles of an excavator were based on the scenario which is often applied in real working conditions. Two driving cycles with respect to the digging and releasing load processes were chosen for calculating the required power, as displayed in Figures 14 and 15. Throughout the maximum and minimum required power, the size and parameters of each device in HPS were reasonably chosen to satisfy the requirement of the system, as listed in Tables 2–4. The operating power of FC was chosen as 55 kW, equal to the average operating power of the system

following the driving cycle shown in Figure 15. The remain power is supplied by BAT and SC. Because SC has higher power density compared to BAT, it is very suitable for the high load mode with high power required. Thus, the operating power that should be chosen should be higher than that of the BAT; thus, the operating power of the SC was 70 kW and the operating power of the BAT was 30 kW.

Table 2. Supercapacitor parameters.

Parameter	Value	Unit
Model	BCAP3000	-
Number of supercapacitors	200	pcs
Rated voltage	2.7	V
Absolute maximum voltage	2.85	V
Absolute maximum current	1900	A
Rated capacitance	3000	F
Maximum capacitance, initial	3600	F
Maximum equivalent series resistance	0.29	mΩ
Total energy	1.458	kW·h

Table 3. Battery parameters.

Parameter	Value	Unit
Capacity	6.5	Ah
Rated voltage	1.2	V
Battery constant voltage	1.2848	V
Internal resistance	0.0046	Ω
Number of batteries	900	pcs
Polarization voltage	0.01875	V
Exponential zone amplitude	0.144	V
Exponential zone time constant inverse	2.3077	$A^{-1} \cdot h^{-1}$
Total energy	7.02	kW·h

Table 4. Fuel cell system parameters.

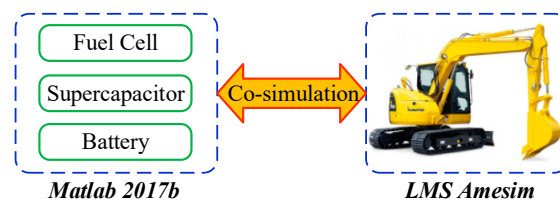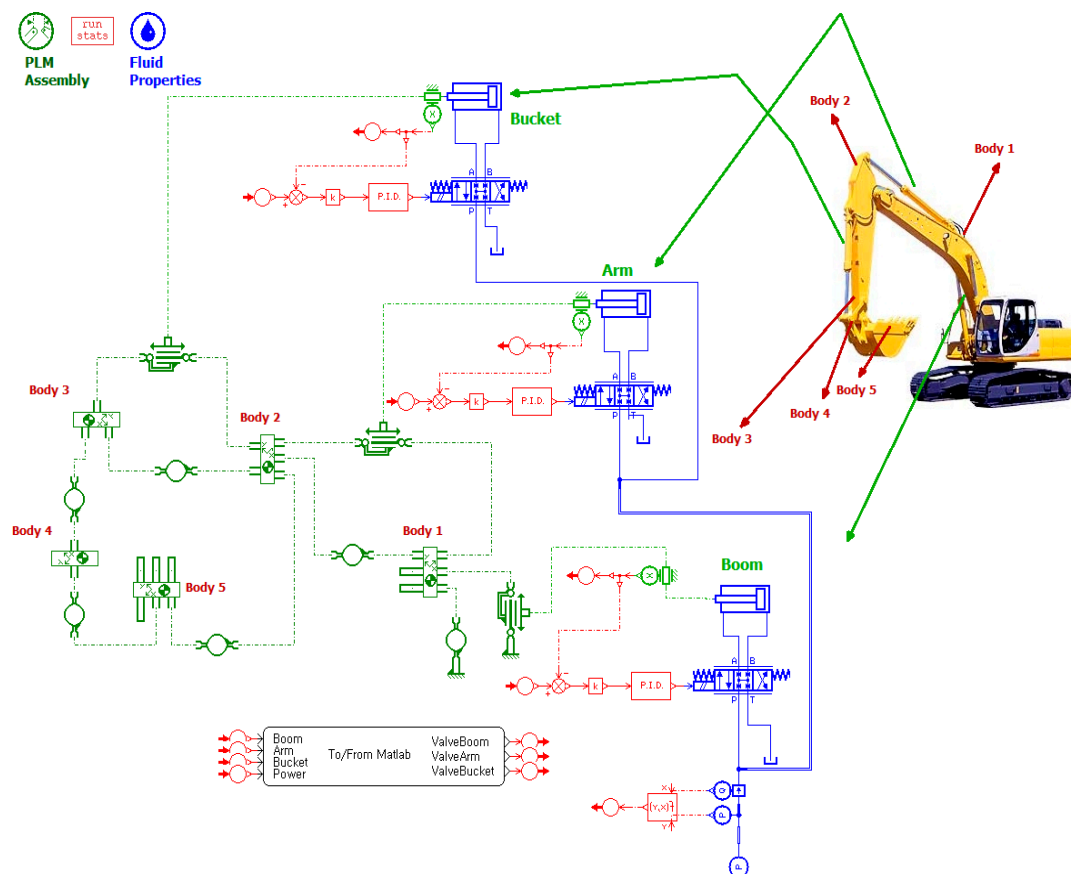| Parameter	Value	Unit
Number of cells	35	pcs
Number of stacks	18	pcs
Rated power	5	kW
Membrane thickness	178	μm
Anode pressure	3	atm
Cathode pressure	3	atm
Cell area	232	cm^2
Membrane resistivity parameter	12.5	-
Reference potential at unity activity	1.229	V
Hydrogen enthalpy of combustion	285.5	$kJ \cdot mol^{-1}$
Universal gas constant	8.314	$J \cdot mol^{-1} \cdot K^{-1}$
Faraday constant	96,485	$C \cdot mol^{-1}$
Thermal resistance	0.115	$°C \cdot W^{-1}$
Thermal capacitance	17.9	$kJ \cdot °C^{-1}$
Anode volume	0.005	m^3
Anode flow constant	0.065	$mol \cdot s^{-1} \cdot atm^{-1}$
Cathode volume	0.01	m^3
Cathode flow constant	0.065	$mol \cdot s^{-1} \cdot atm^{-1}$
Total energy (for 6 h)	302.522	kW·h

Figure 12. Co-simulation environment.

Figure 13. Excavator AMESim hydraulic model [46].
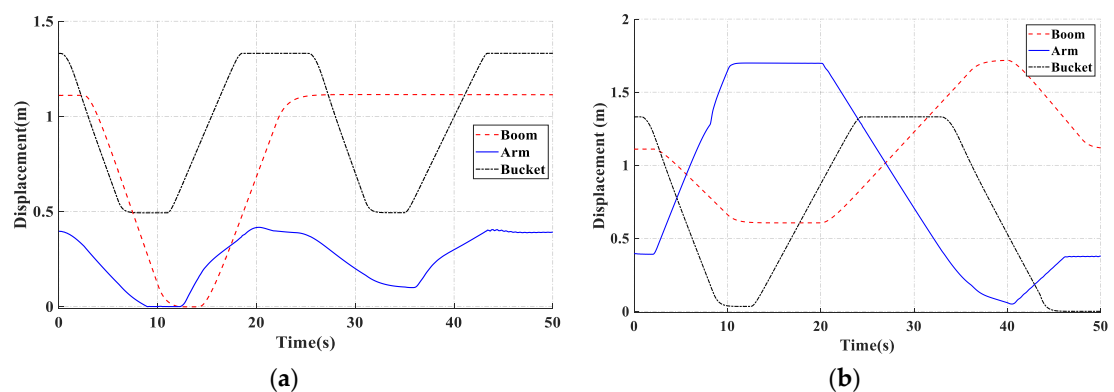

Figure 14. Excavator trajectory of boom, arm, and bucket with two different driving cycles. (**a**) Cycle 1; (**b**) Cycle 2.
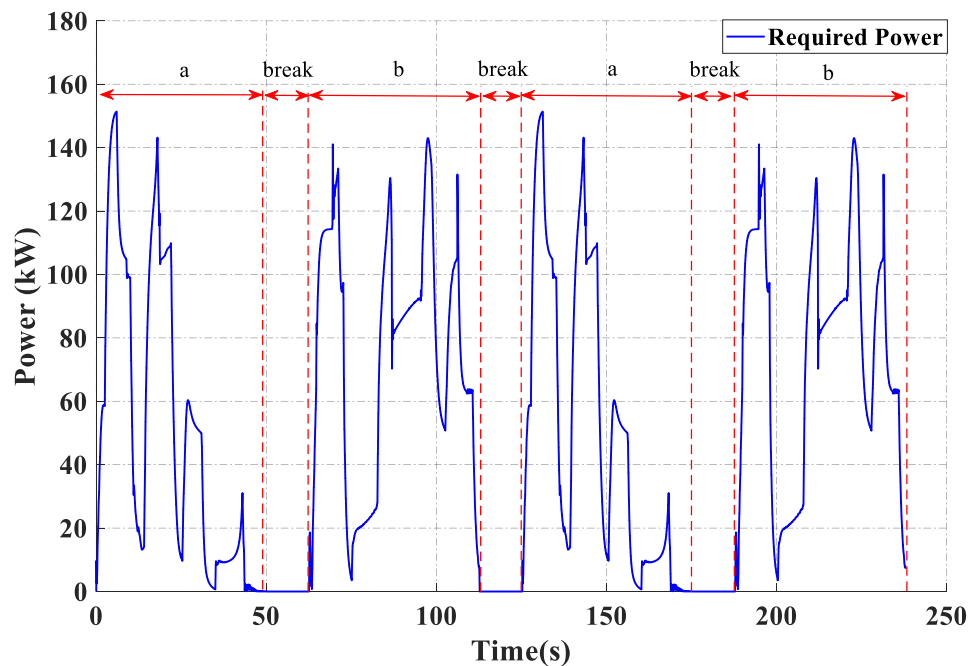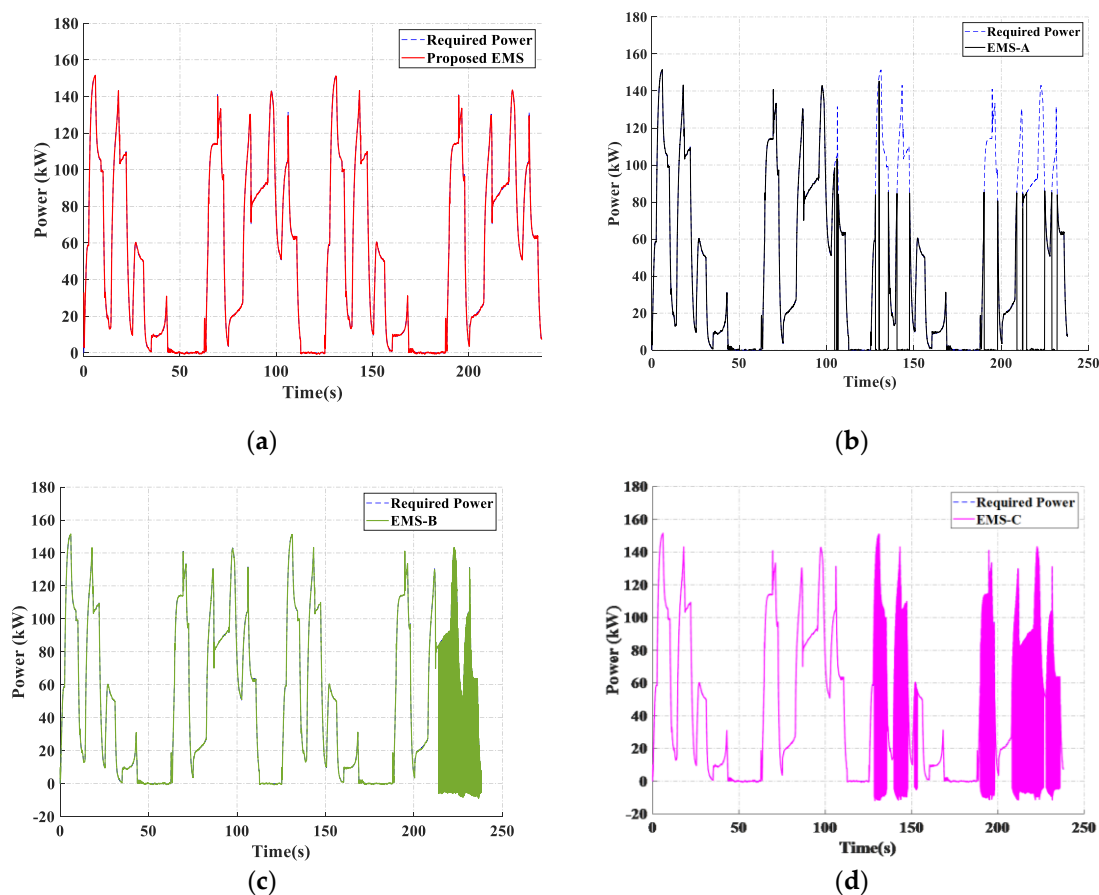
Figure 15. Required power of the excavator with two different working cycles.
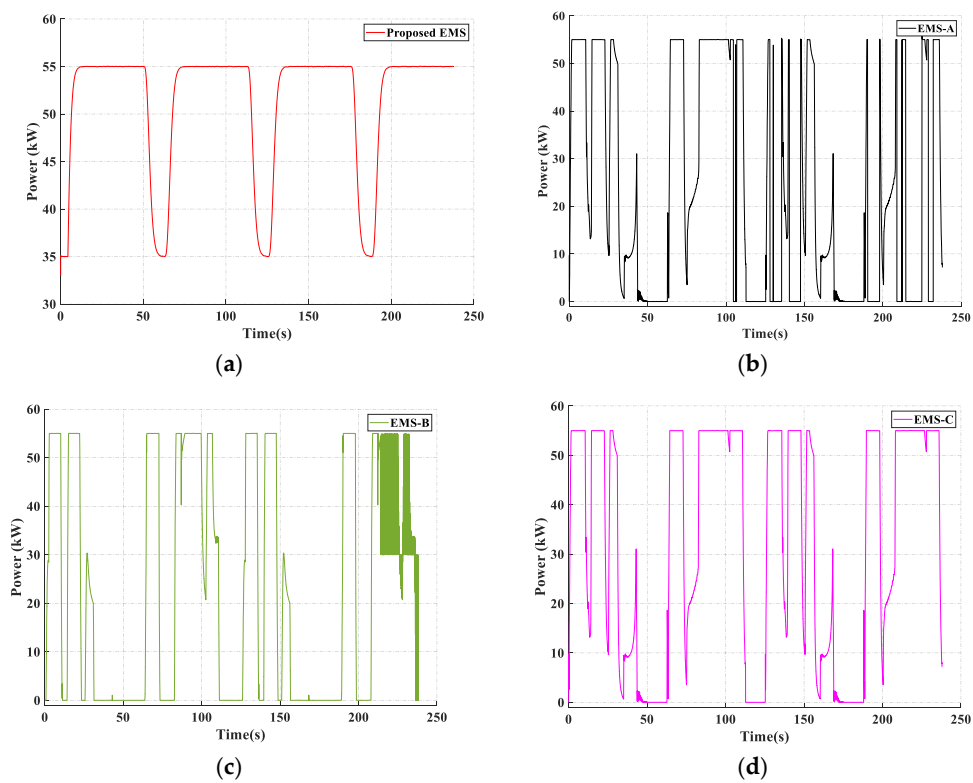
According to Figure 16a, during the two driving cycles, the power supplied by proposed EMS can track the required power well while in the conventional algorithm EMS-A (Figure 16b), the output power of the hybrid power sources cannot supply enough power after 140 s if the required power reaches a high level (i.e., larger than about 95 kW). As can be seen in Figure 17a, based on the energy distribution of the proposed algorithm, the fuel cell stack can be controlled to produce a constant rated power value (55 kW) when the HE is working while in the conventional algorithm EMS-A (Figure 17b), the fuel cell stacks need to run in a varied range due to the variation of the total required power. It can decrease the efficiency of the fuel cell system as well as its lifetime. The initial values of both battery and supercapacitor were set at 0.8 and 0.775 in all EMSs, respectively. As explained in Section 3.1, the conventional algorithm EMS-A does not mention of the charging process. Hence, it did not have enough power when the required power was running in high mode and the SOC_{SC} reached its minimum value of 0.3 at 110 s. As shown in Figure 18b, with only the discharge mode, the SC in the conventional case EMS-A cannot provide any power after 140 s, this causes the problem in the power supply in Figure 16b. While in the proposed EMS, as shown in Figure 18a, the positive values indicate that the SC is in a discharging mode and releasing the power to the excavator whereas negative values mean it is in charging mode and storing energy, then the total power supplied by the HPS can properly track the required power. In the proposed EMS, the battery provides supplementary power during the not very high load demand as shown in Figure 19a; it helps conserve the SC power to use in very high load demand so that the problem will not occur in this case. In the conventional EMS-A (Figure 19b), the battery only provides power after the power of the SC is empty, but it cannot sufficiently supply the needed power due to its low power density characteristic.

For the two HFS-CS (EMS-B) and LCS-CS (EMS-C) strategies, the chattering phenomenon of the power supplied by the HPS occurs at the time 215 s (Figure 16c) and at 145 s and after 180 s (Figure 16d) when the SOC_{SC} (EMS-C in Figure 20) or SOC_{bat} (EMS-B in Figure 21) drops down to the minimum level. Similar with EMS-A, the SOC_{SC} value of EMS-C is also reduced to the minimum value of 0.3 at 130 s while the SOC_{bat} in EMS-B reaches to the minimum value of 0.6 at 210 s. Since the SOC_{bat}/SOC_{sc} hit the minimum level, the devices swiftly switch from discharge to charge mode (Figures 18d and 19c). But after that, when the SOC_{bat}/SOC_{sc} is greater than the minimum level, once again the devices rapidly switch from charging to releasing the power despite low power remaining inside. This progress
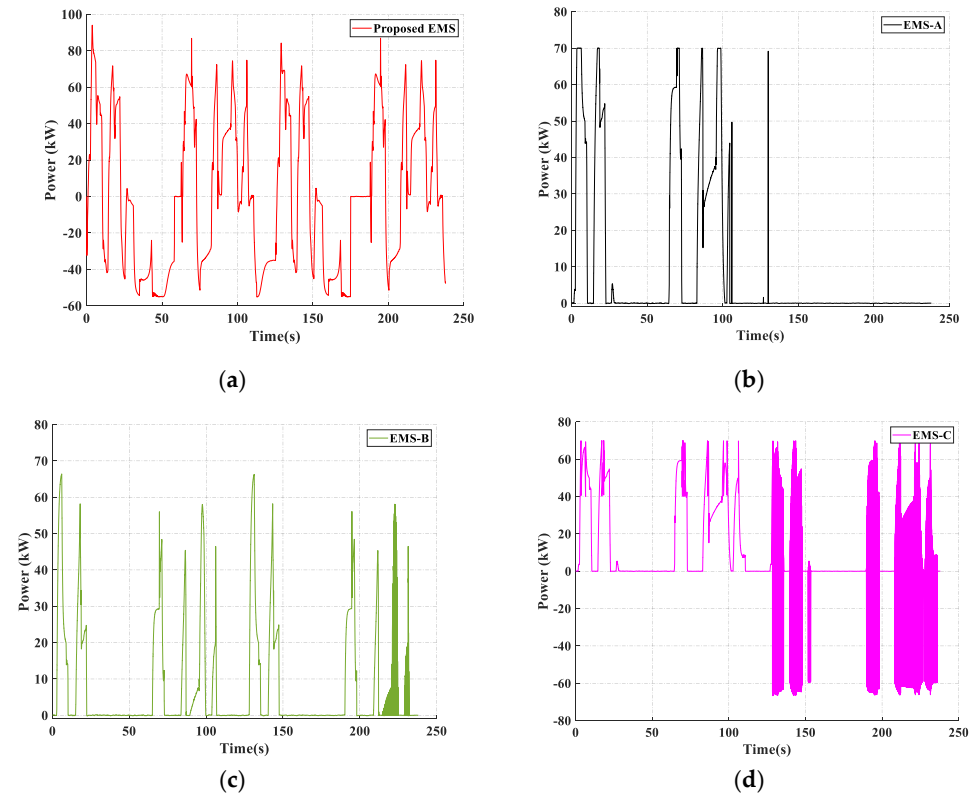
happens repeatedly in Figures 18d and 19c, and oscillation occurs as a result. It also makes the fuel cell run in the chattering condition (as in Figure 17c,d) since the charge and discharge modes are continuously switching to each other. Therefore, these strategies need to be strongly improved since either the system has to temporarily stop for charging as with the conventional algorithm or another strategy is required to maintain the operation. Figure 20; Figure 21 show the effectiveness of the proposed EMS since the states of charge of both storage devices are kept in a suitable working range (60 to 90% for the battery and 30 to 90% for the supercapacitor) which other EMSs cannot achieve. The SOC_{SC} is about 0.85 and the SOC_{bat} is about 0.755 with the proposed EMS. It appears that only the proposed EMS can maintain a reasonably high SOC for both the BAT and SC. It indicates that the proposed EMS is capable of operating for an extended period of time. Also obtained from the above results, the proposed algorithm, which considers all circumstances for stable power-sharing, has better endurance and the supplementary sources are kept in considerably good condition to extend the duration of the requirements.
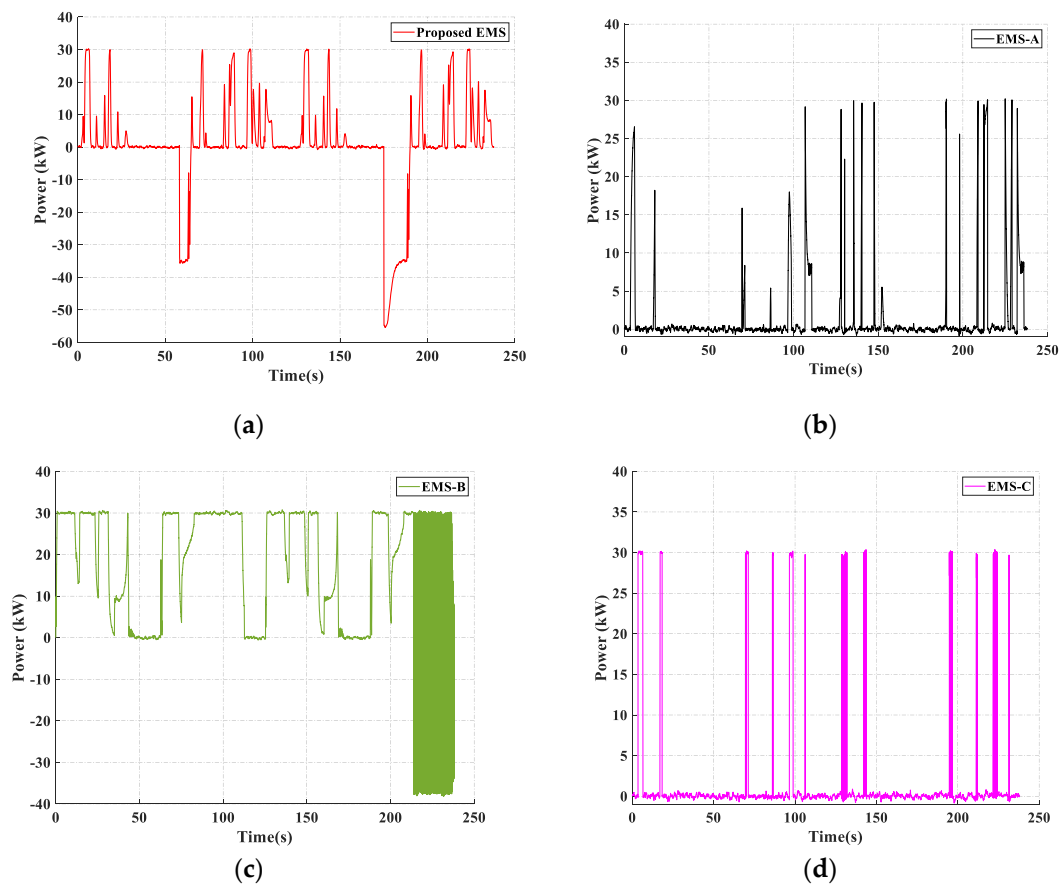

Figure 16. Power response from FC/BAT/SC sources in the proposed case and conventional cases. (**a**) Proposed EMS; (**b**) EMS-A; (**c**) EMS-B; (**d**) EMS-C.
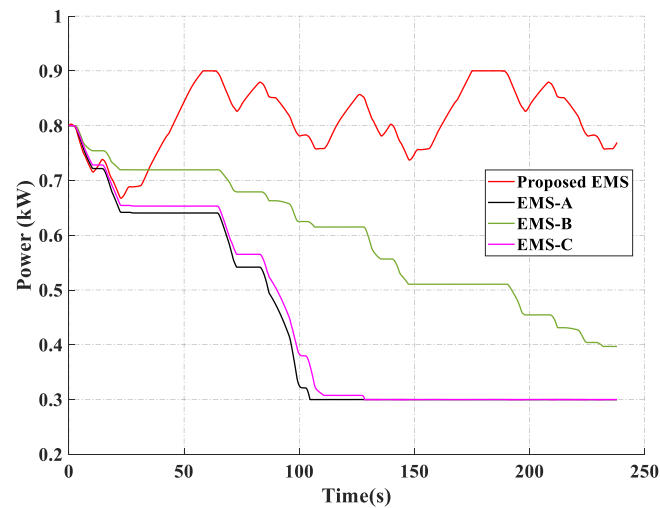
Figure 17. Power from the fuel cell in the proposed case and conventional cases. (**a**) Proposed EMS; (**b**) EMS-A; (**c**) EMS-B; (**d**) EMS-C.

Figure 18. Power from the supercapacitor in the proposed case and conventional cases. (**a**) Proposed EMS; (**b**) EMS-A; (**c**) EMS-B; (**d**) EMS-C.

Figure 19. Power from the battery in the proposed case and conventional cases. (**a**) Proposed EMS; (**b**) EMS-A; (**c**) EMS-B; (**d**) EMS-C.

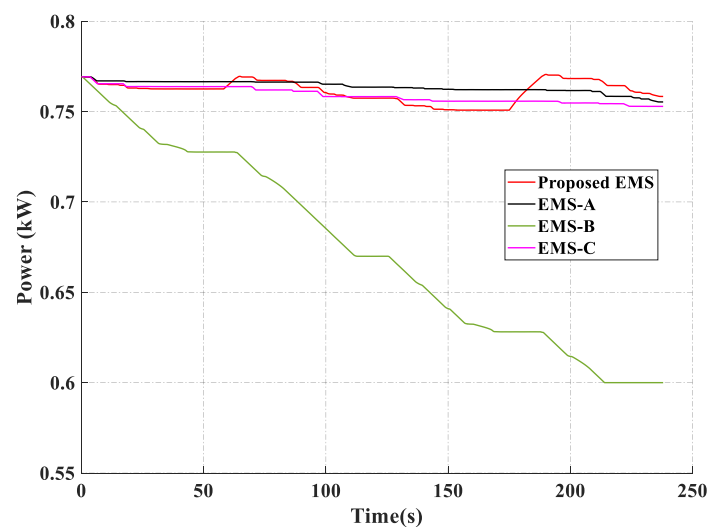**Figure 20.** State of charge of the supercapacitor.

Figure 21. State of charge of the battery.

6. Conclusions

In this paper, the proposed configuration comprising integrated FCs, BATs, and SCs with CEs was firstly presented. A novel energy management system was designed to effectively distribute power from the load demand to all components, keeping the system balanced and dealing with existing drawbacks in the previous works. Different from previous approaches, this configuration used the FC as the main supply for most cases and the BATs/SCs were considered as buffers to extend the working time. The merit of this paper can be considerably summarized as follows:

1. Instead of using one auxiliary device until it is out of power and using the remaining one later, the energy from the powertrain is shared suitably for all devices depending on the load demand and the SOC of each component. Besides, less variation in the power supply from the fuel cell helps to extend its lifespan and maintain its good performance.

2. Due to primarily using power induced from the FC, the BATs/SCs do not need to release too much energy to match the requirement. This allows all supplementary sources to maintain their SOC in good condition.

The simulation results show that the system can satisfy the load demand in comparison with other conventional strategies. However, the power distribution laws in this study are designed based on simple working principles which should be studied in depth. Furthermore, the generation procedure in the CEs is also important due to the complicated structure involved and needs to be considerably investigated. Therefore, the contributions in this study give a new concept and offer future development potential which not only guarantees power supply performance and prolongs the power sources' lifetimes, but also minimizes hydrogen consumption for the hybrid electric construction excavator.

Author Contributions: K.K.A. was the supervisor providing funding and administrating the project, and he reviewed and edited the manuscript. T.C.D., H.V.A.T., H.V.D. carried out the investigation, methodology, analysis, and validation, made the MATLAB and AME Sim software, and wrote the original manuscript. C.M.H. and X.D.T. carried out the simulations and checked the structure of the paper. T.D.D. checked the manuscript and supported the model for research. All authors contributed to this article and accepted the final report.

Conflicts of Interest: The authors declare no conflict of interest.

References

1. Casoli, P.; Riccò, L.; Campanini, F.; Bedotti, A. Hydraulic Hybrid Excavator—Mathematical Model Validation and Energy Analysis. *Energies* **2016**, *9*, 1002. [CrossRef]

2.   Wang, H.; Huang, Y.; Khajepour, A.; He, H.; Cao, D. A novel energy management for hybrid off-road vehicles without future driving cycles as a priori. *Energy* **2017**, *133*, 929–940. [CrossRef]

3.   Truong, D.Q.; Marco, J.; Greenwood, D.; Harper, L.; Corrochano, D.G.; Yoon, J.I. Challenges of micro/mild hybridisation for construction machinery and applicability in UK. *Renew. Sustain. Energy Rev.* **2018**, *91*, 301–320. [CrossRef]

4.   Zhang, J.; Li, Y.; Xu, B.; Chen, X.; Pan, M. Churning losses analysis on the thermal-hydraulic model of a high-speed electro-hydrostatic actuator pump. *Int. J. Heat Mass Transf.* **2018**, *127*, 1023–1030. [CrossRef]

5.   Wang, H.; Wang, Q.; Hu, B. A review of developments in energy storage systems for hybrid excavators. *Autom. Constr.* **2017**, *80*, 1–10. [CrossRef]

6.   Yoon, J.I.; Truong, D.Q.; Ahn, K.K. A generation step for an electric excavator with a control strategy and verifications of energy consumption. *Int. J. Precis. Eng. Manuf.* **2013**, *14*, 755–766. [CrossRef]

7.   Le Hanh, D.; Ahn, K.K.; Kha, N.B.; Jo, W.K. Trajectory control of electro-hydraulic excavator using fuzzy self tuning algorithm with neural network. *J. Mech. Sci. Technol.* **2009**, *23*, 149–160. [CrossRef]

8.   Yoon, J.I.; Kwan, A.K.; Truong, D.Q. A study on an energy saving electro-hydraulic excavator. In Proceedings of the 2009 ICCAS-SICE, Fukuoka, Japan, 18–21 August 2009; IEEE: Piscataway, NJ, USA, 2009; pp. 3825–3830.

9.   Yu, Y.-X.; Ahn, K.K. Optimization of energy regeneration of hybrid hydraulic excavator boom system. *Energy Convers. Manag.* **2019**, *183*, 26–34. [CrossRef]

10. Yu, Y.-X.; Ahn, K.K. Improvement of Energy Regeneration for Hydraulic Excavator Swing System. *Int. J. Precis. Eng. Manuf.-Green Technol.* **2019**, 1–15. [CrossRef]

11. Yu, Y.-X.; Ahn, K.K. Energy Regeneration and Reuse of Excavator Swing System with Hydraulic Accumulator. *Int. J. Precis. Eng. Manuf.-Green Technol.* **2019**, 1–15. [CrossRef]

12. Yi, H.-S.; Jeong, J.-B.; Cha, S.-W.; Zheng, C.-H. Optimal component sizing of fuel cell-battery excavator based on workload. *Int. J. Precis. Eng. Manuf.-Green Technol.* **2018**, *5*, 103–110. [CrossRef]

13. Li, T.; Huang, L.; Liu, H. Energy management and economic analysis for a fuel cell supercapacitor excavator. *Energy* **2019**, *172*, 840–851. [CrossRef]

14. Hannan, M.A.; Azidin, F.A.; Mohamed, A. Multi-sources model and control algorithm of an energy management system for light electric vehicles. *Energy Convers. Manag.* **2012**, *62*, 123–130. [CrossRef]

15. Marzougui, H.; Amari, M.; Kadri, A.; Bacha, F.; Ghouili, J. Energy management of fuel cell/battery/ultracapacitor in electrical hybrid vehicle. *Int. J. Hydrogen Energy* **2017**, *42*, 8857–8869. [CrossRef]

16. Fathabadi, H. Novel fuel cell/battery/supercapacitor hybrid power source for fuel cell hybrid electric vehicles. *Energy* **2018**, *143*, 467–477. [CrossRef]

17. Hames, Y.; Kaya, K.; Baltacioglu, E.; Turksoy, A. Analysis of the control strategies for fuel saving in the hydrogen fuel cell vehicles. *Int. J. Hydrogen Energy* **2018**, *43*, 10810–10821. [CrossRef]

18. Kaya, K.; Hames, Y. Two new control strategies: For hydrogen fuel saving and extend the life cycle in the hydrogen fuel cell vehicles. *Int. J. Hydrogen Energy* **2019**, *44*, 18967–18980. [CrossRef]

19. Paladini, V.; Donateo, T.; de Risi, A.; Laforgia, D. Super-capacitors fuel-cell hybrid electric vehicle optimization and control strategy development. *Energy Convers. Manag.* **2007**, *48*, 3001–3008. [CrossRef]

20. Gherairi, S. Hybrid Electric Vehicle: Design and Control of a Hybrid System (Fuel Cell/Battery/Ultra-Capacitor) Supplied by Hydrogen. *Energies* **2019**, *12*, 1272. [CrossRef]

21. Odeim, F.; Roes, J.; Heinzel, A. Power Management Optimization of an Experimental Fuel Cell/Battery/Supercapacitor Hybrid System. *Energies* **2015**, *8*, 6302–6327. [CrossRef]

22. Dang, T.D.; Do, T.C.; Truong, H.V.A.; Ho, C.M.; Dao, H.V.; Xiao, Y.Y.; Jeong, E.; Ahn, K.K. Design, Modeling and Analysis of a PEM Fuel Cell Excavator with Supercapacitor/Battery Hybrid Power Source. *J. Drive Control* **2019**, *16*, 45–53.

23. Fares, D.; Chedid, R.; Panik, F.; Karaki, S.; Jabr, R. Dynamic programming technique for optimizing fuel cell hybrid vehicles. *Int. J. Hydrogen Energy* **2015**, *40*, 7777–7790. [CrossRef]

24. Xie, S.; Hu, X.; Xin, Z.; Brighton, J. Pontryagin's Minimum Principle based model predictive control of energy management for a plug-in hybrid electric bus. *Appl. Energy* **2019**, *236*, 893–905. [CrossRef]

25. Fu, Z.; Li, Z.; Si, P.; Tao, F. A hierarchical energy management strategy for fuel cell/battery/supercapacitor hybrid electric vehicles. *Int. J. Hydrogen Energy* **2019**, *44*, 22146–22159. [CrossRef]

26. Bambang, R.T.; Rohman, A.S.; Dronkers, C.J.; Ortega, R.; Sasongko, A. Energy management of fuel cell/battery/supercapacitor hybrid power sources using model predictive control. *IEEE Trans. Ind. Inform.* **2014**, *10*, 1992–2002.

27. Khan, M.J.; Iqbal, M.T. Modelling and Analysis of Electro-chemical, Thermal, and Reactant Flow Dynamics for a PEM Fuel Cell System. *Fuel Cells* **2005**, *5*, 463–475. [CrossRef]

28. Sankar, K.; Aguan, K.; Jana, A.K. A proton exchange membrane fuel cell with an airflow cooling system: Dynamics, validation and nonlinear control. *Energy Convers. Manag.* **2019**, *183*, 230–240. [CrossRef]

29. Musio, F.; Tacchi, F.; Omati, L.; Gallo Stampino, P.; Dotelli, G.; Limonta, S.; Brivio, D.; Grassini, P. PEMFC system simulation in MATLAB-Simulink®environment. *Int. J. Hydrogen Energy* **2011**, *36*, 8045–8052. [CrossRef]

30. Pukrushpan, J.T. *Modeling and Control of Fuel Cell Systems and Fuel Processor*; Department of Mechanical Engineering, The University of Michigan: Ann Arbor, MI, USA, 2003.

31. Erdinc, O.; Vural, B.; Uzunoglu, M. A wavelet-fuzzy logic based energy management strategy for a fuel cell/battery/ultra-capacitor hybrid vehicular power system. *J. Power Sources* **2009**, *194*, 369–380. [CrossRef]

32. Uzunoglu, M.; Alam, M.S. Dynamic modeling, design and simulation of a PEM fuel cell/ultra-capacitor hybrid system for vehicular applications. *Energy Convers. Manag.* **2007**, *48*, 1544–1553. [CrossRef]

33. Zhang, L.; Hu, X.; Wang, Z.; Sun, F.; Dorrell, D.G. A review of supercapacitor modeling, estimation, and applications: A control/management perspective. *Renew. Sustain. Energy Rev.* **2018**, *81*, 1868–1878. [CrossRef]

34. Zubieta, L.; Bonert, R. Characterization of double-layer capacitors for power electronics applications. *IEEE Trans. Ind. Appl.* **2000**, *36*, 199–205. [CrossRef]

35. Lahyani, A.; Venet, P.; Guermazi, A.; Troudi, A. Battery/Supercapacitors Combination in Uninterruptible Power Supply (UPS). *IEEE Trans. Power Electron.* **2013**, *28*, 1509–1522. [CrossRef]

36. Gualous, H.; Bouquain, D.; Berthon, A.; Kauffmann, J.M. Experimental study of supercapacitor serial resistance and capacitance variations with temperature. *J. Power Sources* **2003**, *123*, 86–93. [CrossRef]

37. Ham, H.; Han, K.; Lee, H. Battery System Modeling for a Military Electric Propulsion Vehicle with a Fault Simulation. *Energies* **2013**, *6*, 5168–5181. [CrossRef]

38. Sockeel, N.; Shi, J.; Shahverdi, M.; Mazzola, M. Sensitivity Analysis of the Battery Model for Model Predictive Control: Implementable to a Plug-In Hybrid Electric Vehicle. *World Electr. Veh. J.* **2018**, *9*, 45. [CrossRef]

39. Sockeel, N.; Shahverdi, M.; Mazzola, M.; Meadows, W. High-Fidelity Battery Model for Model Predictive Control Implemented into a Plug-In Hybrid Electric Vehicle. *Batteries* **2017**, *3*, 13. [CrossRef]

40. Tremblay, O.; Dessaint, L.-A.; Dekkiche, A.-I. A generic battery model for the dynamic simulation of hybrid electric vehicles. In Proceedings of the 2007 IEEE Vehicle Power and Propulsion Conference, Arlington, TX, USA, 9–12 September 2007; IEEE: Piscataway, NJ, USA, 2007; pp. 284–289.

41. Castaings, A.; Lhomme, W.; Trigui, R.; Bouscayrol, A. Practical control schemes of a battery/supercapacitor system for electric vehicle. *IET Electr. Syst. Transp.* **2016**, *6*, 20–26. [CrossRef]

42. Dinh, T.X.; Thuy, L.K.; Tien, N.T.; Dang, T.D.; Ho, C.M.; Truong, H.V.A.; Dao, H.V.; Do, T.C.; Ahn, K.K. Modeling and Energy Management Strategy in Energetic Macroscopic Representation for a Fuel Cell Hybrid Electric Vehicle. *J. Drive Control* **2019**, *16*, 80–90.

43. Nguyen, B.; German, R.; Trovão, J.P.F.; Bouscayrol, A. Real-Time Energy Management of Battery/Supercapacitor Electric Vehicles Based on an Adaptation of Pontryagin's Minimum Principle. *IEEE Trans. Veh. Technol.* **2019**, *68*, 203–212. [CrossRef]

44. Ge, L.; Quan, L.; Zhang, X.; Zhao, B.; Yang, J. Efficiency improvement and evaluation of electric hydraulic excavator with speed and displacement variable pump. *Energy Convers. Manag.* **2017**, *150*, 62–71. [CrossRef]

45. Oh, K.-S.; Seo, J.-H. Inertial Parameter Estimation of an Excavator with Adaptive Updating Rule Using Performance Analysis of Kalman Filter. *Int. J. Control Autom. Syst.* **2018**, *16*, 1226–1238. [CrossRef]

46. Siemens LMS AMESim AME Sim Help: Example. Available online: https://www.plm.automation.siemens.com/global/en/search.html?query=help&lang=en (accessed on 15 November 2019).